Title: Comparison of objective functions for batch crystallization using a simple process model and Pontryagin's minimum principle

Authors: Yu-Ti Tseng, Jeffrey D. Ward

PII: S0098-1354(17)30017-0
DOI: http://dx.doi.org/doi:10.1016/j.compchemeng.2017.01.017
Reference: CACE 5673

To appear in: *Computers and Chemical Engineering*

Received date: 24-6-2016
Revised date: 9-1-2017
Accepted date: 11-1-2017

Please cite this article as: Tseng, Yu-Ti., & Ward, Jeffrey D., Comparison of objective functions for batch crystallization using a simple process model and Pontryagin's minimum principle.*Computers and Chemical Engineering* http://dx.doi.org/10.1016/j.compchemeng.2017.01.017

Highlights

- Optimal, nearly-analytical trajectories for batch crystallization are determined.
- Nine objective functions are considered for three case study systems.
- Process model includes only crystal nucleation and simple growth.
- Nearly-analytical results facilitate comparison of objectives.

Comparison of objective functions for batch crystallization using a simple process model and Pontryagin's minimum principle

Yu-Ti Tseng and Jeffrey D. Ward*

Dept. of Chemical Engineering, National Taiwan University, Taipei 106-07, Taiwan

Abstract

In this contribution different objective functions based on the moments of the product crystal size distribution are compared using optimal control theory to solve for the optimal batch trajectory for each objective. For a simple crystallization process model with only nucleation and ordinary crystal growth, and neglecting the contribution of the nucleated mass to the nucleation rate and material balance, mostly analytic expressions are obtained for the optimal control vector. Different objective functions lead to different final values for the costates, which lead to different sets of coupled differential and algebraic equations which must be solved to determine the values of constants numerically. The results of nine different objective functions for three crystal systems are presented. The objective functions based on the lower moment of the nucleated crystals lead to late-growth trajectories while the objective functions based on the higher moment of the nucleated crystals lead to early-growth trajectories, consistent with previous findings. The effect of seed loading is also investigated.

Topical Heading: Particle Technology and Fluidization

Keywords: batch crystallization, Pontryagin's minimum principle, optimal control theory

* fax: +886-2-2369-1314, e-mail jeffward@ntu.edu.tw

1. Introduction

Batch crystallization is an important and widely-used operation in chemical engineering for the separation and purification of solid products. The quality of crystalline products is primarily determined by the crystal polymorph, crystal shape and crystal size distribution. Achieving a desired or optimal product crystal size distribution is important for many applications in industrial crystallization and has been the subject of considerable study. Most of the research on the operation of batch crystallization has focused on the question of how the supersaturation (which may depend on the batch temperature, evaporation rate or rate of anti-solvent addition) should change with time during the batch to maximize or minimize the value of some objective function.

Because the supersaturation changes continuously during the batch, the problem is a continuous optimization problem. The most widely-used method for solving this problem is control vector parameterization (Kraft, 1985; Schlegel et al., 2005), which has been applied to solve a number of complicated problems including optimization with aggregation (O'Ciardha et al., 2012), crystal shape evolution (Acevedo, et al., 2015; Liu et al., 2013; Ma et al., 2002), enantiomer separation (Angelov et al., 2008) polymorphic phase transition (Sheikholeslamzadeh and Rohani, 2013), simultaneous cooling and antisolvent addition (Nagy et al., 2008) and imperfect mixing (Ma et al., 2002). Several review articles (Nagy and Braatz, 2012; Nagy et al., 2013) discuss control of batch crystallization more generally.

A number of researchers have applied Pontryagin's minimum principle to determine optimal trajectories for batch crystallization over the years (Jones 1974; Ajinkya and Ray 1974; Morari 1980; Corriou and Rohani 2008). Raisch and coworkers (Vollmer and Raisch 2003; Vollmer and Raisch 2006; Hofmann and Raisch, 2010; Bajcinca et al., 2010) proposed a transformation of the standard method of moments model which permits a nearly analytical solution to the optimal control problem to be determined for a simple crystallization process

model including only nucleation and ordinary growth (no size-dependent growth or growth-rate dispersion). The nearly analytical nature of the result permits greater understanding of the nature of the solution than was previously possible. For example, they proved mathematically that when certain relationships hold between parameters in the nucleation and growth kinetic models and the objective function is to minimize the nucleated mass, the growth rate trajectory always passes through a minimum and reaches the maximum constraint near the end of the batch. Further extensions and applications of the method were presented by Bajcinca and coworkers (Bajcinca and Hofmann 2011; Bajcinca 2013).

An important consideration in the formulation of any optimization problem is the selection of objective function, and this is particularly true for batch crystallization, where subtle differences in the choice of objective function can have a significant effect on the outcome (Chung et al, 1999; Ma et al, 2002; Ward et al, 2006; Hsu and Ward, 2013). In some instances, the best choice for the objective function will be clear because of regulatory requirements or other factors, but in other instances the engineer must choose the objective function using his or her own best judgement. Although it is not the only possibility, most researchers formulate objective functions based on the moments of the crystal size distribution.

Chung et al. (1999) and Ma et al., (2002) were among the first to call attention to the effect of the objective function on the results of the optimization in batch crystallization processes. They considered several different objective functions, including some that were based on lower moments of the crystal size distribution and others that were based on higher moments of the crystal size distribution and found significantly different trajectories for different objective functions. Ward et al. (2006) surveyed objective functions considered by different authors and argued that objective functions based on lower moments of the nucleated mass lead to so-called early growth trajectories, while those based on higher moments of the

nucleated crystals or any moment of the seed-grown crystals lead to late-growth trajectories. Later, Hsu and Ward (2013) compared the results of using different objective functions and argued that minimizing the nucleated mass was the most appropriate objective function in most circumstances, but in that work the optimization problem was solved using control vector parameterization and therefore the results were entirely numerical.

Besides the effect the supersaturation trajectory, researchers have also investigated the effect of seed loading (Jagadesh et al., 1999; Kubota et al., 2001; Doki et al., 2002; Hojjati and Rohani, 2005; Tseng and Ward, 2014). Generally increasing the seed mass and decreasing the seed size is found to improve performance, and in some cases nucleation can be suppressed almost entirely by suitable seeding.

In the present contribution, the method of Hofmann and Raisch (2010) is applied to determine nearly-analytical expressions for the optimal supersaturation trajectory in seeded batch crystallization for nine different objective functions. Because the results are mostly analytical, they can be more readily understood and compared. Because the choice of objective function has a profound effect on the results of the optimization, it is necessary for the engineer to understand the effect of the choice of objective function on the resulting supersaturation trajectory and product crystal size distribution. Without this understanding, the engineer may choose an objective function that leads to an undesirable result.

The remainder of this article is organized as follows: In the next section, some mathematical theory related to batch crystallization processes and optimization is reviewed, including a brief summary of the method of Hofmann and Raisch and modifications necessary to solve the problem for different objective functions. In the third section, results are presented. Comparison is made between the optimal trajectories for different objective functions for three different crystallization systems, and the effect of seed loading is also investigated. Finally, conclusions are presented in the final section.

2. Theory

In this section a model for a batch crystallization process is introduced, the method of Hofmann and Raisch is briefly reviewed and modifications necessary to consider different objective functions are presented. Results are illustrated using three complete batch crystallization models taken from the literature: a model for the crystallization of potassium nitrate from water by Miller and Rawlings (1994) (also used by Chung et al. (1999)), a model for the crystallization of succinic acid from water by Qiu et al. (1991) and a model for the crystallization of pentaerythritol from water by Bernardo et al (2010).

2.1 Batch crystallization model

In this work a standard moment model that describes a batch crystallization system is considered:

$$\frac{d\mu_0}{dt} = B \tag{1}$$

$$\frac{d\mu_i}{dt} = iG\mu_{i-1} \quad i = 1,2,... \tag{2}$$

Where G is size independent crystal growth rate (m/s) and B is nucleation rate (#/m^{3}s). The definition of the moments is:

$$\mu_i = \int_0^\infty L^i f(L) dL \quad i = 0,1,2... \tag{3}$$

The driving force for crystal nucleation and growth is the supersaturation. The relative supersaturation is given by:

$$S = \frac{C - C_{sat}}{C_{sat}} \tag{4}$$

where C and C_{sat} are the solute concentration and saturation solute concentration in units of kg/kg solvent. The following empirical expressions can be employed for the nucleation and growth rates:

$$G = k_g S^g \tag{5}$$

$$B = k_b S^b \mu_3^{\ j} \tag{6}$$

where μ_3 is the third moment of crystal size distribution. An expression for a mass balance on the solute is

$$\frac{dC}{dt} = -3G\rho_c k_v \mu_2 \tag{7}$$

For the seed-grown crystals (subscript s) and nuclei-grown crystals (subscript n), the expressions are:

$$\frac{d\mu_{s,0}}{dt} = 0 \tag{8}$$

$$\frac{d\mu_{s,i}}{dt} = iG\mu_{s,i-1} \quad i = 1, 2, ... \tag{9}$$

$$\frac{d\mu_{n,0}}{dt} = B \tag{10}$$

$$\frac{d\mu_{n,i}}{dt} = iG\mu_{n,i-1} \quad i = 1, 2, ... \tag{11}$$

Note that for each moment, the total crystal value equals the seed-grown value plus nuclei-grown value:

$$\mu_{T,i} = \mu_{n,i} + \mu_{s,i} \tag{12}$$

The initial values of the moments are given by:

$$\mu_{i,s}(0) = \mu_{i0,s}\,; \quad \mu_{i,n}(0) = 0\,; \tag{13}$$

Throughout this work the crystal size distribution of the seeds is assumed to be a parabolic distribution of the following form:

$$f(L) = a(L - L_0(1-w))(L + L_0(1-w))\,; \quad w = 0.2; \tag{14}$$

Where a is constant, L_0 is the mean size and w is the width of the parabolic distribution. Model parameters for the three case studies considered in this work are given in Table 1.

The model developed in this section and used in this work is quite minimalistic; it describes a crystallization process with only nucleation and ordinary, temperature-independent growth (no size-dependent growth or growth-rate dispersion) and does not account for breakage, aggregation, changes in particle shape or other factors that may influence a crystallization process. These restrictions are necessary to obtain the nearly-analytical solutions that are presented in Section 3. Results based on this model can be used to understand processes in which the dominant tradeoff encountered in process operation is between nucleation and ordinary growth, but should be used with caution if other phenomena have a significant effect on the product CSD.

2.2 Objective Functions

As stated previously, although some objectives such as D90 and D10 cannot be expressed in terms of the moments of the crystal size distribution, the most widely-used objective functions for batch crystallization are based on the moments. Table 2 lists nine possible objective functions, all of which are based on the moments of the product crystal size distribution (either moments of the nucleated crystals or moments of the combined nucleated and seed-grown crystals). It may be desirable to minimize the weight mean coefficient of variation or the number mean coefficient of variation of the product crystals, or to maximize the weight mean size or number mean size of the product crystals, or to minimize the number of nuclei or the nucleated mass. Minimizing the first, second or fourth moment of the nucleated mass is seldom considered in the literature, but these possibilities are included for completeness and to investigate trends. It is also possible to construct additional objective functions using linear combinations of the objective functions given in Table 2.

2.3 Transformation and optimal control problem formulation

In this section, the method of Hoffman and Raisch (2010) is briefly reviewed. Readers are referred to their paper for additional details. A useful general reference for optimal control

theory and Pontryagin's minimum principle is the textbook by Lewis et al. (2012). A transformed time τ is defined as:

$$d\tau = G(t)dt \tag{15}$$

The control input *u* is the inverse of the growth rate:

$$u(\tau) = \frac{1}{G(\tau)} \tag{16}$$

The real time *t* in terms of τ is tracked by the following equation:

$$\frac{dt}{d\tau} = \frac{1}{G(\tau)} \tag{17}$$

The states of the system are defined as follows:

$$\begin{aligned} &x_1 = \mu_{5,n}\,; \quad x_2 = \mu_{4,n}\,; \quad x_3 = \mu_{3,n}\,; \\ &x_4 = \mu_{2,n}\,; \quad x_5 = \mu_{1,n}\,; \quad x_6 = \mu_{0,n}\,; \quad x_7 = t\,; \end{aligned} \tag{18}$$

Bounds on the control input are established as follows:

$$u = \left[\left(\frac{1}{G}\right)_{\min}, \left(\frac{1}{G}\right)_{\max} \right] \tag{19}$$

The bounds of control input *u* are related to the lower and upper limits on the supersaturation. These bounds should be set in a reasonable range that the process is operated in the metastable zone. The key simplification is to neglect the effect of the nucleated mass on the nucleation rate, i.e. to assume that

$$B(G, \mu_{3,T}) \approx B(G, \mu_{3,s}) \tag{20}$$

This assumption is necessary to achieve the analytical results presented later, but it should be treated with caution. The assumption is most reasonable when the nucleated mass is small compared to the seed-grown mass (which is the desired condition) but it may introduce considerable error if the nucleated mass is significant compared to the seed-grown mass. With these definitions and assumptions the differential equations for the states of the system can be written:

$$\frac{dx_1}{d\tau}=5x_2,\quad \frac{dx_2}{d\tau}=4x_3,\quad \frac{dx_3}{d\tau}=3x_4,\quad \frac{dx_4}{d\tau}=2x_5,\quad \frac{dx_5}{d\tau}=x_6 \tag{21}$$

$$\frac{dx_6}{d\tau}=\frac{B}{G}\left(\mu_{3,s}(\tau),u(\tau)\right) \tag{22}$$

$$\frac{dx_7}{d\tau}=u(\tau) \tag{23}$$

The boundary conditions for the states are

$$\mathbf{x}(0)=\mathbf{0};\quad x_7\left(\tau_f\right)=t_{f,\mathrm{c}} \tag{24}$$

An expression for $\frac{B}{G}$ in terms of *u* can also be derived:

$$\frac{B\left(u(\tau)\right)}{G\left(u(\tau)\right)}=k_b k_g^{-\frac{b}{g}}u(\tau)^{\frac{g-b}{g}}\,\mu_{3,s}(\tau)^j \tag{25}$$

In this work nine different objective functions are considered. They are listed in Table 2. All objective functions considered here are in terms of the final state and does not include integral terms. In general the optimization problem can be stated as:

$$\min_{u(\tau)}.\ \phi\left(\mu_{i,\mathrm{n}}\left(\tau_f\right)\right)\ \text{s.t.}\quad \begin{aligned} t\left(\tau_f\right)&=t_{f,\mathrm{c}}\\ \mu_{3,\mathrm{s}}\left(\tau_f\right)&=\mu_{3,f,\mathrm{s},c}\\ u(\tau)&\in U\ \forall\ \tau\in[0,\tau_f] \end{aligned} \tag{26}$$

The Hamiltonian matrix is:

$$\begin{aligned} H\left(\mathbf{x},u,\boldsymbol{\psi},\tau\right)&=\boldsymbol{\psi}^{\mathrm{T}}\frac{d}{d\tau}\mathbf{x}\\ &=5\psi_1x_2+4\psi_2x_3+3\psi_3x_4+4\psi_4x_5\\ &\quad+\psi_5x_6+\psi_6\frac{B}{G}\left(\mu_{3,s}(\tau),u(\tau)\right)+\psi_7u \end{aligned} \tag{27}$$

The differential equations of the costate (or the adjoint state) are $\frac{d}{d\tau}\boldsymbol{\psi}=-\frac{\partial}{\partial\mathbf{x}}H$:

$$\begin{aligned}
&\frac{d}{d\tau}\psi_1 = 0 \\
&\frac{d}{d\tau}\psi_2 = -5\psi_1,\ \frac{d}{d\tau}\psi_3 = -4\psi_2,\ \frac{d}{d\tau}\psi_4 = -3\psi_3,\ \frac{d}{d\tau}\psi_5 = -2\psi_4,\ \frac{d}{d\tau}\psi_6 = -\psi_5 \\
&\frac{d}{d\tau}\psi_7 = 0,
\end{aligned} \tag{28}$$

A necessary conditions for an optimal trajectory is that the optimal control input $u^*(\tau)$ must satisfy

$$\begin{aligned}
u^*(\tau) &= \underset{u\in U}{\operatorname{argmin}} H(\mathbf{x}, u, \boldsymbol{\psi}, \tau) \\
&= \underset{u\in U}{\operatorname{argmin}} \psi_6 \frac{B}{G}\left(\mu_{3,s}(\tau), u(\tau)\right) + \psi_7 u
\end{aligned} \tag{29}$$

The following candidate for an unconstrained minimizer can be found by setting the partial derivative of *H* with respect to *u* equal to zero:

$$\begin{aligned}
\frac{\partial}{\partial u} H\Big|_{u^0} &= -\psi_6 \frac{b-g}{g} k_b k_g^{-\frac{b}{g}} \left(u^0\right)^{-\frac{b}{g}} \mu_{3,s}^j(\tau) + \psi_7 = 0 \\
u^0 &= \frac{1}{k_g}\left(\frac{\psi_6}{\psi_7}\frac{b-g}{g} k_b \mu_{3,s}^j(\tau)\right)^{\frac{g}{b}}
\end{aligned} \tag{30}$$

2.4 Final values of costates for different objective functions

If there is no constraint on the terminal value of a state variable x_i, then the final value of the corresponding costate variable ψ_i in Equation 28 is given by:

$$\psi_i(\tau_f) = \frac{\partial \phi}{\partial x_{i,f}} \tag{31}$$

There is a constraint on the final value of x_7, therefore the final value of ψ_7 remains free, but the final values of $\psi_1 - \psi_6$ depend on the objective function considered. Hoffmann and Raisch (2010) used the nucleated mass as the objective function, i.e. $\phi\left(\mu_{i,\mathrm{n}}(\tau_f)\right) = \mu_{3,\mathrm{n}}(\tau_f)$. In this work nine different objective functions are considered. In this section expressions for the final values of the costates and resulting expressions for the costates as functions of τ are derived

for two objective functions to illustrate the procedure that was used in this work. When the objective is to minimize the number of nuclei, i.e. $\phi\left(\mu_{i,\mathrm{n}}\left(\tau_f\right)\right)=\mu_{0,\mathrm{n}}\left(\tau_f\right)$, the final values of the costates are determined as follows:

$$\phi\left(\mathbf{x_f},\tau_f\right)=x_{6f};\quad \frac{\partial\phi}{\partial x_{6f}}=1;\ \Rightarrow\ \psi_6\left(\tau_f\right)=1 \tag{32}$$

The final values of the other moments $\mu_{1,n}\left(\tau_f\right)$, $\mu_{2,n}\left(\tau_f\right)$, $\mu_{3,n}\left(\tau_f\right)$ and $\mu_{4,n}\left(\tau_f\right)$ are neither part of the cost function nor part of the constraints. Therefore the following result is obtained:

$$\frac{\partial\phi}{\partial x_{i,f}}=0;\quad i=1,2,3,4,5;\quad \Rightarrow\psi_1\left(\tau_f\right)=\psi_2\left(\tau_f\right)=\psi_3\left(\tau_f\right)=\psi_4\left(\tau_f\right)=\psi_5\left(\tau_f\right)=0 \tag{33}$$

With the final values of the costates $\psi_i\left(\tau_f\right)$ listed above, expressions for the values of the costates as functions of τ are determined by solving Equation 28:

$$\begin{aligned}
\psi_1(\tau)&=0\\
\psi_2(\tau)&=0\\
\psi_3(\tau)&=0\\
\psi_4(\tau)&=0\\
\psi_5(\tau)&=0\\
\psi_6(\tau)&=k_1\\
\psi_7(\tau)&=k_2
\end{aligned} \tag{34}$$

Where k_1 is equal to 1 as mentioned in Equation 32 and k_2 is computed by integrating $\frac{dx_7}{d\tau}=u(\tau)$.

For the objective that minimizes the weight mean coefficient of variation (WMCOV) the final values of the costates are determined as follows:

$$
\begin{aligned}
&\phi\left(\mathbf{x_f},\tau_f\right)=\sqrt{\frac{\mu_{3T,f}\mu_{5T,f}}{\mu_{4T,f}^2}-1}\,;\\
&\frac{\partial\phi}{\partial x_{1f}}=\psi_1\left(\tau_f\right)=\frac{1}{2\sqrt{\frac{\mu_{3T,f}\mu_{5T,f}}{\mu_{4T,f}^2}-1}}\times\frac{\mu_{3T,f}}{\mu_{4T,f}^2};\\
&\frac{\partial\phi}{\partial x_{2f}}=\psi_2\left(\tau_f\right)=\frac{1}{2\sqrt{\frac{\mu_{3T,f}\mu_{5T,f}}{\mu_{4T,f}^2}-1}}\times\frac{\mu_{5T,f}\mu_{3T,f}}{\mu_{4T,f}^3};\\
&\frac{\partial\phi}{\partial x_{3f}}=\psi_3\left(\tau_f\right)=\frac{1}{2\sqrt{\frac{\mu_{3f}\mu_{5f}}{\mu_{4f}^2}-1}}\times\frac{\mu_{5f}}{\mu_{4f}^2};
\end{aligned}
\tag{35}
$$

$$
\frac{\partial\phi}{\partial x_{i,f}}=0;\quad i=4,5,6;\quad\Rightarrow\psi_4\left(\tau_f\right)=\psi_5\left(\tau_f\right)=\psi_6\left(\tau_f\right)=0
\tag{36}
$$

The following expressions for the values of the costates are then obtained:

$$
\begin{aligned}
&\psi_1(\tau)=k_1\\
&\psi_2(\tau)=-5k_1(\tau-\tau_f)+k_2\\
&\psi_3(\tau)=10k_1(\tau-\tau_f)^2-4k_2(\tau-\tau_f)+k_3\\
&\psi_4(\tau)=-10k_1(\tau-\tau_f)^3+6k_2(\tau-\tau_f)^2-3k_3(\tau-\tau_f)\\
&\psi_5(\tau)=5k_1(\tau-\tau_f)^4-4k_2(\tau-\tau_f)^3+3k_3(\tau-\tau_f)^2\\
&\psi_6(\tau)=-k_1(\tau-\tau_f)^5+k_2(\tau-\tau_f)^4-k_3(\tau-\tau_f)^3\\
&\psi_7(\tau)=k_4
\end{aligned}
\tag{37}
$$

Where the constants are

$$
\begin{aligned}
k_1&=\frac{1}{2\sqrt{\frac{\mu_{3T,f}\mu_{5T,f}}{\mu_{4T,f}^2}-1}}\times\frac{\mu_{3T,f}}{\mu_{4T,f}^2}\\
k_2&=\frac{-1}{\sqrt{\frac{\mu_{3T,f}\mu_{5T,f}}{\mu_{4T,f}^2}-1}}\times\frac{\mu_{5T,f}\mu_{3T,f}}{\mu_{4T,f}^3}\\
k_3&=\frac{1}{2\sqrt{\frac{\mu_{3T,f}\mu_{5T,f}}{\mu_{4T,f}^2}-1}}\times\frac{\mu_{5T,f}}{\mu_{4T,f}^2}
\end{aligned}
\tag{38}
$$

And the constant k_4 is computed by integrating $\frac{dx_7}{d\tau}=u(\tau)$.

In the case of more complicated objective functions such as this one, it is not possible to solve for the constants k_i independently. In such cases, the values of the constants were determined using the numerical non-linear equation-solving routine *fsolve* in Matlab. Given a residuals function, this routine searches for the values of the arguments that make the outputs of the residuals function equal to zero. The residuals function is constructed as follows. It accepts as inputs values of the constants k_i. Given these values, the values of the costates as a function of τ are given by Equation 37 and so Equations 21–23 can be integrated and the constants k_i can be calculated based on the values of the moments at the end of the batch. Finally, the residuals which are to be made equal to zero are calculated as the initial values of the constants minus the calculated values of the constants. To test for the possibility of multiple solutions, for each case the routine was started from several different initial conditions and was always found to converge to the same solution.

Because the candidate minimizer (Eq. 30) depends only on ψ_6 and ψ_7, it is only necessary to determine these values in order to integrate Equations 21–23. Table 3 lists the expressions for ψ_6 and ψ_7 in terms of τ and constants as well as expressions for each constant in terms of the final moments of the crystal size distribution for every objective function considered in this work.

3. Results

3.1 Potassium nitrate system

The optimal input trajectories for all nine objective functions for the potassium nitrate process are shown in Figure 1. Because the control input is the reciprocal of the growth rate ($1/G$), it can be seen from the figure that three objectives, the number mean coefficient of variation (NMCOV), number mean size (NMS) and the number of nuclei (mu0n) lead to early growth trajectories, because the growth rate is highest at the beginning of the batch and

decreases over the course of the batch. For NMCOV and NMS, the trajectory is constrained at the beginning of the batch (the growth rate is equal to the maximum allowed value at the beginning of the batch) while for mu0n the trajectory is always unconstrained. The remaining trajectories can all be considered to be late-growth trajectories as they reach the growth rate constraint at the end of the batch, although they all have a minimum in the growth rate in the middle of the batch. Comparing the trajectories for objectives mu1n–mu4n, as the order of the moment of the nucleated mass used in the objective function increases, the minimum in the growth rate occurs earlier and the growth rate constraint is also reached earlier. Figure 2 shows the corresponding crystal growth rate versus time for each trajectory. All of the trajectories except that of mu0n require very rapid changes in the crystal growth rate which would be difficult to achieve in practice.

Figure 3 shows the crystal number size distribution of the nucleated crystals for each trajectory. Only the nucleated crystal size distribution is shown because the seed product crystal distribution is the same for all objective functions. The dashed black line represents the number size distribution that would be achieved if the process was operated at the maximum allowed growth rate for the entire batch. Because the larger crystals are those that were formed earlier in the batch, the volume size distribution for the nucleated crystals lies on the constraint for larger crystal size if it lies on the constraint in the time (or τ) domain at the beginning of the batch, i.e. for NMS and NMCOV. Conversely it lies on the constraint for smaller crystal size if it lies on the constraint at the end of the batch in the time domain, i.e. for all other objectives except mu0n.

Figure 4 shows the volume size distributions corresponding to the number size distributions shown in Figure 3. Because the trajectories corresponding to the objectives NMS and NMCOV lie on the constraint for large values of the crystal size, they result in a much larger nucleated crystal mass than the other objectives. The objectives mu0n and mu1n also

result in a nucleated mass significantly larger than necessary. Results for objectives mu4n, mu3n, mu2n and WMS are similar and all lead to a small nucleated mass.

As a further check of the validity of the results, the optimization problem was solved again using control vector parameterization with a linear spline. The results were found to be consistent with expectation, i.e. the shape of the optimal trajectory was in each case found to be similar to that determined by the minimum principle, but the value of the objective function was slightly worse in each case due to the representation of the control vector by a spline.

3.2 Pentaerythritol system

Figures 5–8 show the analogous results for the pentaerythritol system. Similar to the potassium nitrate system, the objectives NMS and NMCOV lead to early-growth operating policies and much larger nucleated masses than the other objectives. In the pentaerythritol system the exponent *j* in the nucleation rate expression (Eq. 6) is equal to zero so that the nucleation rate does not depend on the mass of solid crystals in the crystallizer. In this case the growth rate trajectory which minimizes the number of nuclei is just the constant growth rate trajectory (seen most clearly in Figure 5 but also in Figure 6) because if the nucleation rate does not depend on the solid crystal mass there is no advantage from having a higher growth rate at the beginning of the batch when the solid crystal mass is smaller. Also, the number size distribution corresponding to operation on the constraint (the black dashed line in Figure 7) is also a flat distribution because the nucleation rate is constant if the growth rate is constant and the nucleation rate does not depend on the total crystal mass.

3.3 Succinic acid system

Figures 9–12 and 13–16 show the results for the succinic acid system for the cases where the seed mass is 1% and 3.2% of the total seed-grown product yield respectively. Comparing the two sets of figures shows the significant effect that changing the seed loading

can have on the operation of the process and the product crystal size distribution. Generally speaking, since increasing the seed loading with a constant seed size corresponds to increasing the number of seeds, it also corresponds to decreasing the amount of growth required, i.e. decreaseing τ_f, because more solute is absorbed for a given growth rate if more seeds are growing. Because the growth rate, on average, is smaller if the seed loading is larger, the nucleation rate is also smaller and therefore the nucleated mass is smaller as well. Comparing Figure 9 (1% seed loading) and Figure 13 (3.2% seed loading), τ_f is larger when the seed loading is smaller. Furthermore, all of the growth rates are larger ($1/G$ is smaller), and trajectories spend more time on the constraint when the seed loading is smaller. This can also be seen by comparing Figure 10 and Figure 14. The figures for the number size distribution (Figures 11 and 15) and volume size distribution (Figures 12 and 16) also show that both the number of nuclei and the nucleated mass are significantly smaller when the seed loading is larger.

Table 4 shows the resulting value of every objective when each objective is used in the optimization. Each row corresponds to a different objective being applied. For example, when the objective is to minimize the weight COV (wCOV) the resulting value of the weight COV is 0.1704. The trajectory that minimizes the wCOV leads to a number COV (nCOV) of 2.2828 and a weight mean size (WMS) of 0.8787. When the objective is to minimize the nCOV, the resulting value of the nCOV is 0.2983, the value of the wCOV is 0.3209, the value of the WMS is 0.6307 and so on.

Careful inspection of this table shows that any of the objective functions based on the lower moments of the crystal size distribution (nCOV NMS, mu0n) give good results for all objective based on the lower moments, but bad results for all objectives based on the higher moments (wCOV, WMS, mu3n). Conversely any of the objective functions based on the higher moments give good results for all objectives based on the higher moments but bad

results for all objectives based on the lower moments. This shows that there is an inherent tradeoff between optimizing properties of the lower moments and properties of the higher moments. Objectives based on the lower moments lead to early-growth trajectories which give good results for all objectives based on the early moments, while objectives based on the higher moments lead to late-growth trajectories which give good results for all objectives based on the higher moments.

4. Conclusions

In this work, a simple process model including only crystal nucleation and ordinary growth is applied for the optimization of three different crystallization systems using nine different objective functions, subject to the assumption that the contribution of the nucleated mass to the nucleation rate and material balance can be neglected. In all cases, objectives based on higher moments lead to late-growth operating policies and give good results for all objectives based on higher moments but poor results for objectives based on lower moments. This finding is consistent with results reported previously (Ward et al, 2006; Hsu and Ward, 2013). An inherent tradeoff exists between optimizing properties of the lower moments of the product crystal size distribution and the higher moments. Finally, using the number mean size or number coefficient of variation as the objective function can lead to a large nucleated mass and may therefore be undesirable, which is also consistent with previous findings (Ma et al., 2002; Hsu and Ward, 2013).

Acknowledgement

The authors wish to express their gratitude to the National Science Council of Taiwan for financial support.

Notation

B = nucleation rate (#/m^3 s)

C = concentration (kg/m^3)

C_s = seed loading ratio (-)

C_s* = critical seed loading ratio (-)

C_{sat} = saturated concentration (kg/m^3)

f = crystal size distribution function (#/m^3 m)

G = crystal growth rate (m/s)

k_b = nucleation parameter (#/m^3 s)

k_g = growth parameter (m/s)

k_v = volumetric shape factor (-)

L_p = product volume mean size (m)

L_s = seed volume mean size (m)

m_s = seed mass (kg)

n_0 = number of seed crystals (#/m^3)

S = relative supersaturation (-)

t_f = final time (s)

w = solvent mass (kg)

W_s = seed mass (kg)

W_{th} = theoretical crystal yield (kg)

x_0 = seed mean size (m)

μ_i = ith moment of the crystal size distribution (m^i/m^3)

ρ_c = crystal density (kg/m^3)

References

Acevedo, D., Tandy, Y., Nagy, Z. K., 2015. Multiobjective Optimization of an Unseeded Batch Cooling Crystallizer for Shape and Size Manipulation. Ind. Eng. Chem. Res., 54, 2156–2166.

Ajinkya, M. B., Ray, W. H., 1974. On the optimal operation of crystallization processes. Chem. Eng. Comm., 1, 181–186.

Angelov, I., Raisch, J., Elsner, M. P., Seidel-Morgenstern, A., 2008. Optimal operation of enantioseparation by batch-wise preferential crystallization. Chem. Eng. Sci., 63, 1282–1292.

Bajcinca, N., 2013. Analytic solutions to optimal control problems in crystal growth processes. J. Proc. Control, 23, 224241.

Bajcinca, N., Hofmann, S., Raisch, J., Sundmacher, K., 2010. Robust and optimal control scenarios for batch crystallization processes. In Proc. of ESCAPE-20, Ischia, Naples, Italy, 1605–1610.

Bajcinca, N., Hofmann, S., 2011. Optimal control for batch crystallization with size-dependent growth kinetics. In American Control Conference 2011, San Francisco, USA.

Bernardo, A., Giulietti, M., 2010. Modeling of crystal growth and nucleation rates for pentaerythritol batch crystallization. Chem. Eng. Res. & Des. 88, 1356–1364.

Chung, S. H., Ma, D. L., Braatz, R. D., 1999. Optimal seeding in batch crystallization. Can. J. Chem. Eng., 77, 590–596.

Corriou, J. P., Rohani, S., 2008. A new look at optimal control of a batch crystallizer. AIChE J., 54, 3188-3206.

Doki, N., Kubota, N., Yokota, M., Chianese, A., 2002. Determination of critical seed loading ratio for the production of crystals of uni-modal size distribution in batch cooling crystallization of potassium alum. J. Chem. Eng. Jpn., 35, 670-676.

Hofmann, S., Raisch, J., 2010. Application of optimal control theory to a batch crystallizer using orbital flatness. In 16th Nordic Process Control Workshop, Lund, Sweden 25–27.

Hojjati, H., Rohani, S., 2005. Cooling and seeding effect on supersaturation and final crystal size distribution (CSD) of ammonium sulphate in a batch crystallizer. Chem. Eng. Processing, 44, 949-957.

Hsu, C. W., Ward, J. D., 2013. The Best Objective Function for Seeded Batch Crystallization. AIChE J., 59, 390398.

Jagadesh, D., Kubota, N., Yokota, M., Doki, N., Sato, A., 1999. Seeding effect on batch crystallization of potassium sulfate under natural cooling mode and a simple design method of crystallizer. J. Chem. Eng. Jpn., 32, 514–520.

Jones, A. G., 1974. Optimal operation of a batch cooling crystallizer. Chem. Eng. Sci., 29, 1075–1087.

Kraft, D. (1985). On Converting Optimal Control Problems into Nonlinear Programming Problems. In K. Schittkowski (Ed.), Computational Mathematical Programming (pp. 261-280). Berlin, Heidelberg: Springer Berlin Heidelberg.

Kubota, N., Doki, N., Yokota, M., Sato, A., 2001. Seeding policy in batch cooling crystallization. Powder Technol., 121, 3138.

Lewis, F. L., Vrabie, D. L., Syrmos, V. L. (2012). Optimal control (3rd ed.). Hoboken: Wiley.

Liu, J. J., Hu, Y. D., Wang, X. Z., 2013. Optimization and control of crystal shape and size in protein crystallization process. Comput. Chem. Eng., 57, 133140.

Ma, D. L., Tafti, D. K., Braatz, R. D., 2002. Optimal control and simulation of multidimensional crystallization processes. Comput. Chem. Eng., 26, 1103–1116.

Miller, S. M., Rawlings, J. B., 1994. Model identification and control strategies for batch cooling crystallizers. AIChE Journal, 40, 1312–1327.

Morari, M., 1980. Some comments on the optimal operation of batch crystallizers. Chem. Eng. Comm., 4, 167–171.

Nagy, Z. K., Braatz, R. D., 2012. Advances and New Directions in Crystallization Control. Annual Review of Chemical and Biomolecular Engineering, Vol 3, 3, 55–75.

Nagy, Z. K., Fevotte, G., Kramer, H., Simon, L. L., 2013. Recent advances in the monitoring, modelling and control of crystallization systems. Chem. Eng. Res. Des., 91, 1903–1922.

Nagy, Z. K., Fujiwara, M., Braatz, R. D., 2008. Modelling and control of combined cooling and antisolvent crystallization processes. J. of Proc. Control, 18, 856-864.

O'Ciardha, C. T., Hutton, K. W., Mitchell, N. A., Frawley, P. J., 2012. Simultaneous Parameter Estimation and Optimization of a Seeded Antisolvent Crystallization. Crystal Growth & Design, 12, 5247–5261.

Qiu, Y. F., Rasmuson, A. C., 1991. Nucleation and Growth of Succinic Acid in a Batch Cooling Crystallizer. AIChE Journal, 37, 1293–1304.

Schlegel, M., Stockmann, K., Binder, T., Marquardt, W., 2005. Dynamic optimization using adaptive control vector parameterization. Computers & Chemical Engineering, 29, 1731-1751.

Sheikholeslamzadeh, E., Rohani, S., 2013. Modeling and Optimal Control of Solution Mediated Polymorphic Transformation of L-Glutamic Acid. Ind. Eng. Chem. Res., 52, 2633–2641.

Tseng, Y. T., Ward, J. D., 2014. Critical seed loading from nucleation kinetics. AIChE J., 60, 1645–1653.

Vollmer, U., Raisch, J., 2003. Control of batch cooling crystallization processes based on orbital flatness. Int. J. Control, 76, 1635–1643.

Vollmer, U., Raisch, J., 2006. Control of batch crystallization - A system inversion approach. Chem. Eng. Process., 45, 874–885.

Ward, J. D., Mellichamp, D. A., Doherty, M. F., 2006. Choosing an operating policy for seeded batch crystallization. AIChE Journal, 52, 2046–2054.

Figures

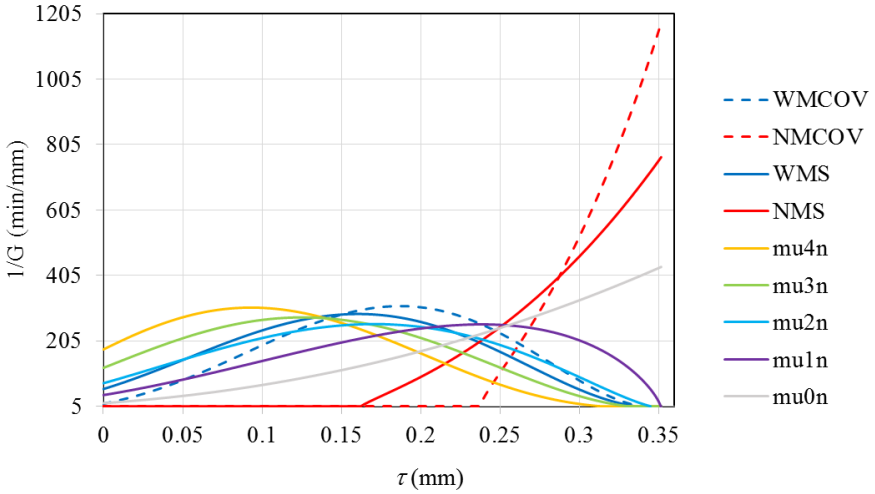

Figure 1. Control input (u^0) in τ domain for potassium nitrate system.

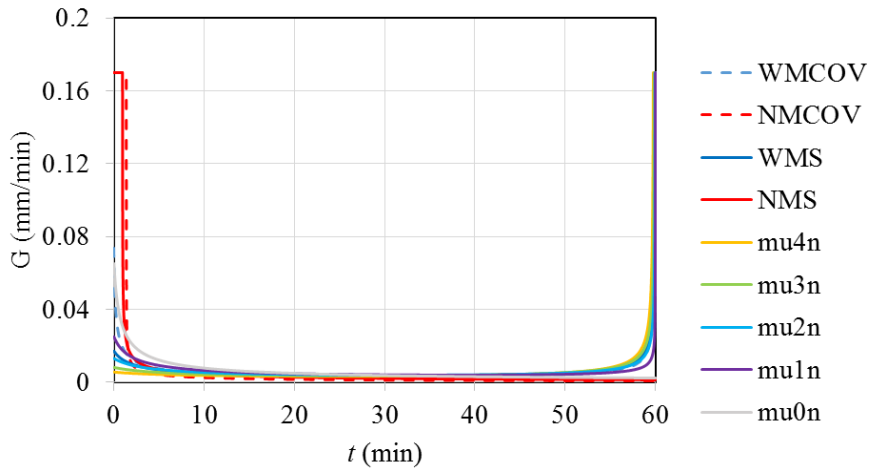

Figure 2. Growth rate in time domain for potassium nitrate system.

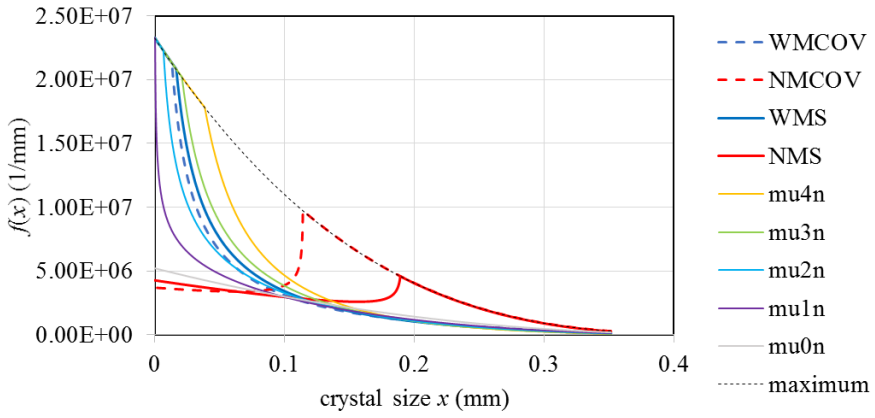

Figure 3. Crystal size distribution of the nucleus crystal for potassium nitrate system.

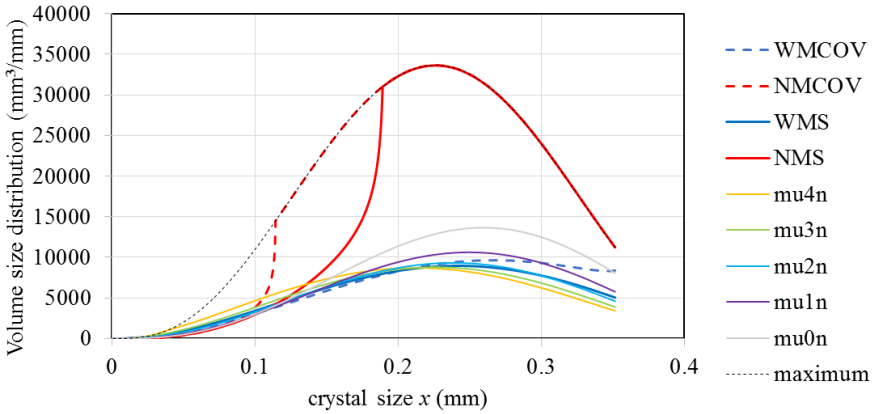

Figure 4. Volume size distribution of the nucleus crystal for potassium nitrate system.

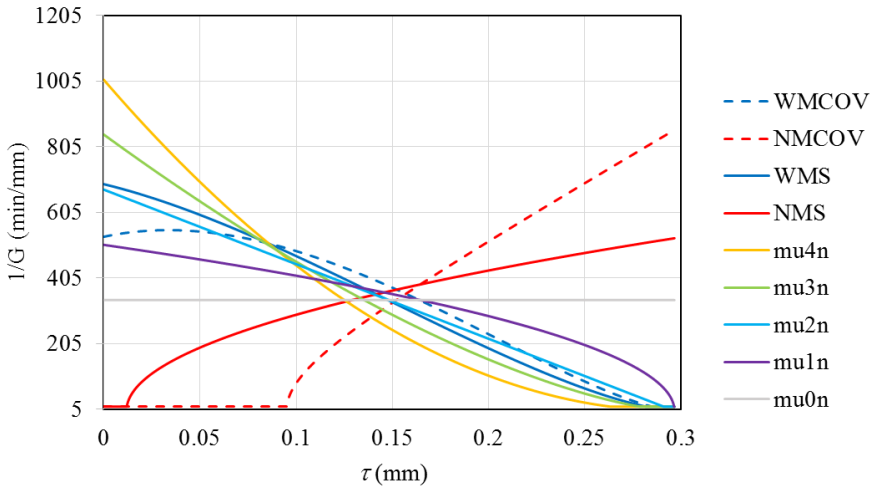

Figure 5. Control input (u^0) in τ domain for pentaerythritol system.

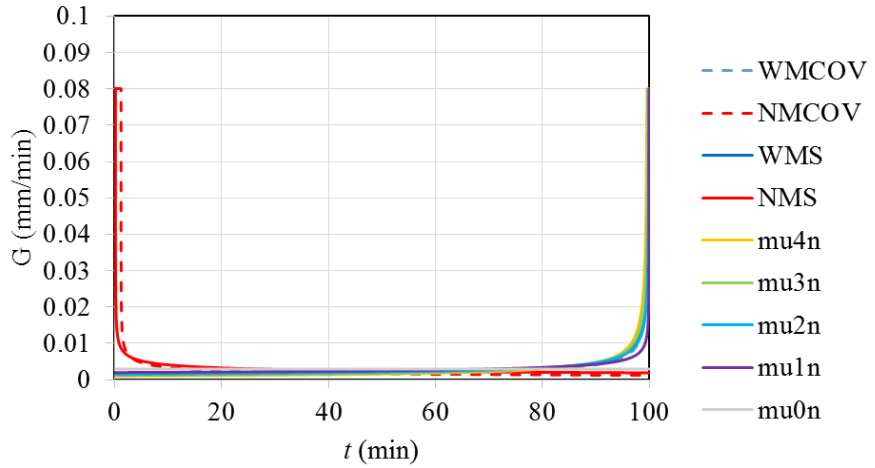

Figure 6. Growth rate in time domain for pentaerythritol system.

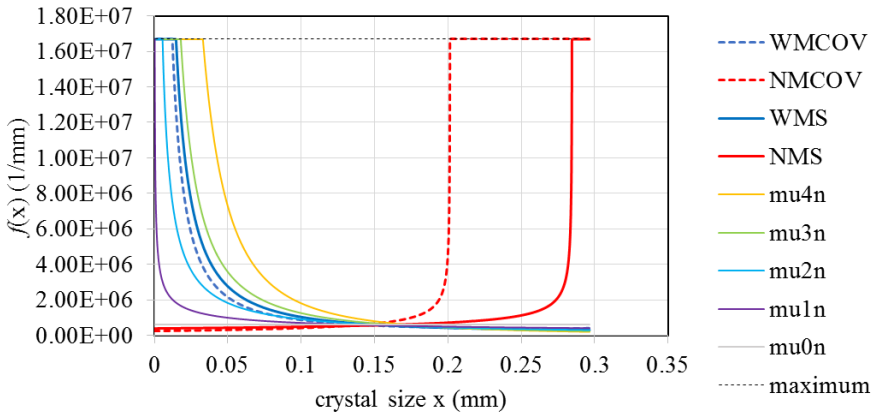

Figure 7. Crystal size distribution of the nucleus crystal for pentaerythritol system.

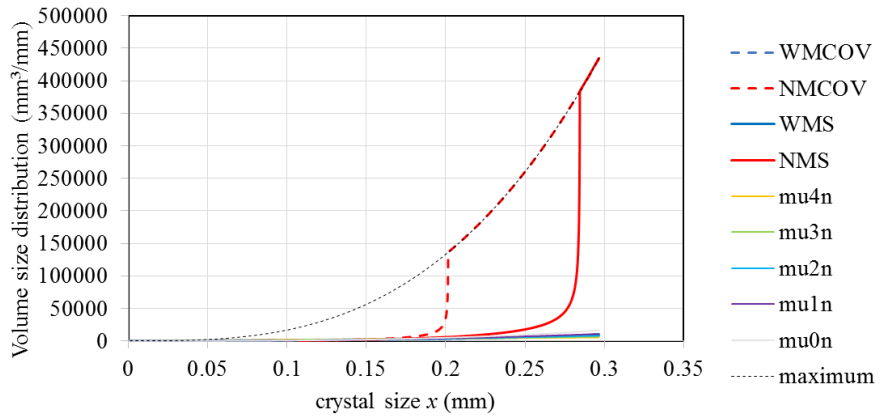

Figure 8. Volume size distribution of the nucleus crystal for pentaerythritol system.

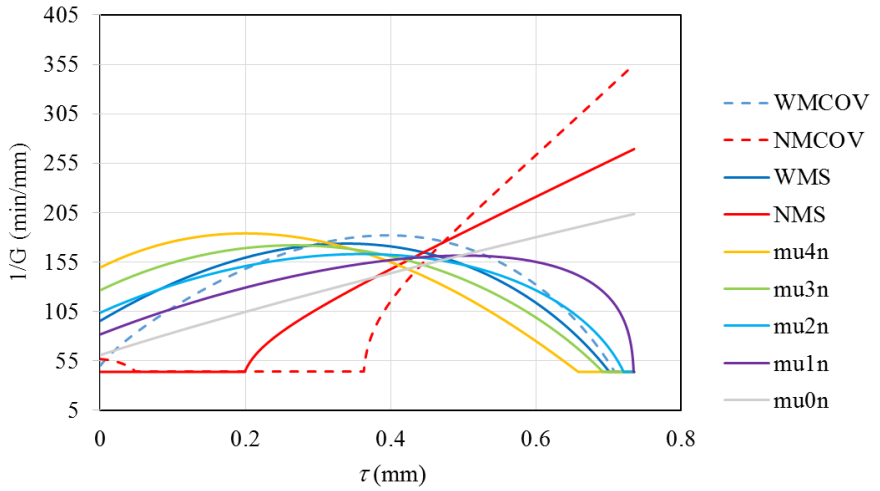

Figure 9. Control input (u^0) in τ domain for succinic acid system (1% seed loading).

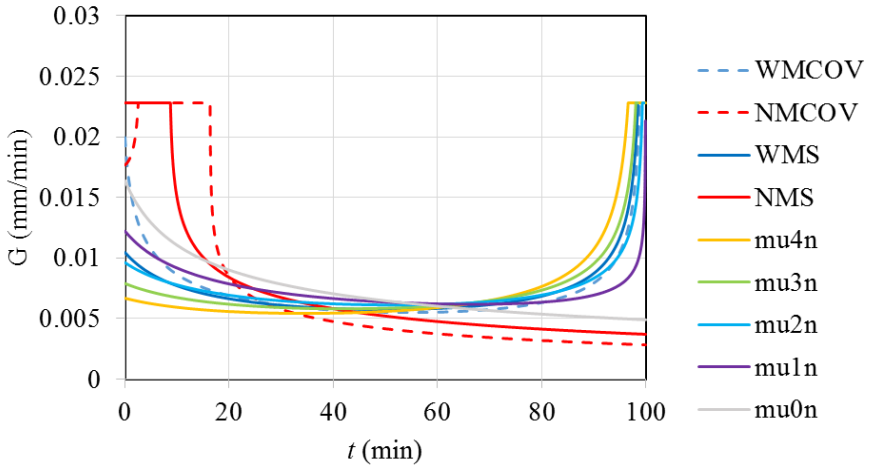

Figure 10. Growth rate in time domain for succinic acid system (1% seed loading).

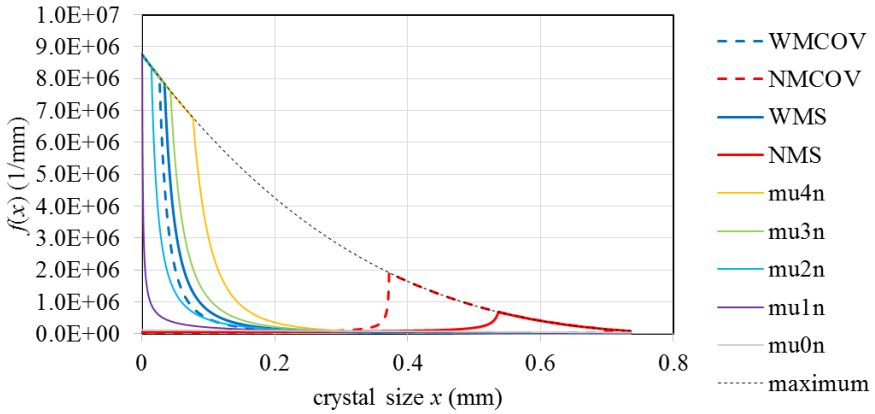

Figure 11. Crystal size distribution of the nucleus crystal for succinic acid system (1% seed loading).

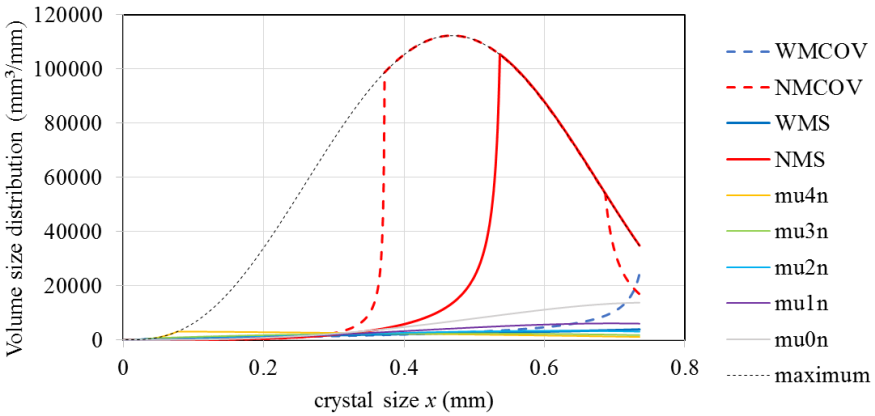

Figure 12. Volume size distribution of the nucleus crystal for succinic acid system (1% seed loading).

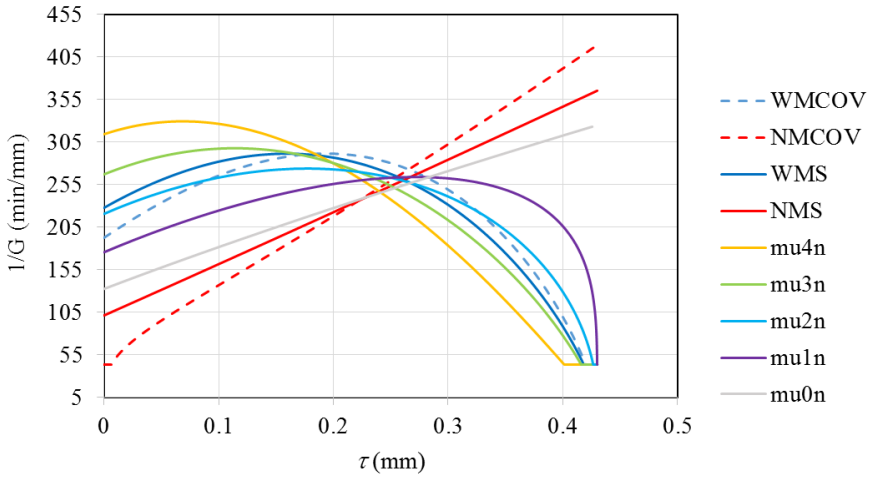

Figure 13. Control input (u^0) in τ domain for succinic acid system (3.2% seed loading).

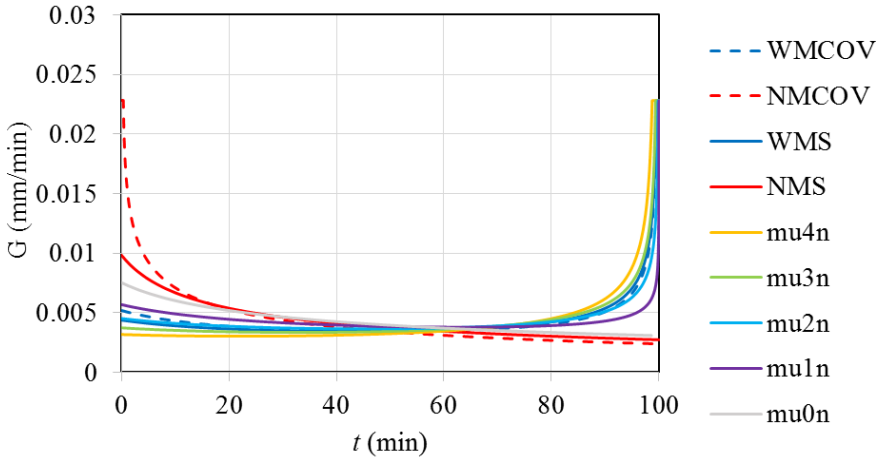

Figure 14. Growth rate in time domain for succinic acid system (3.2% seed loading).

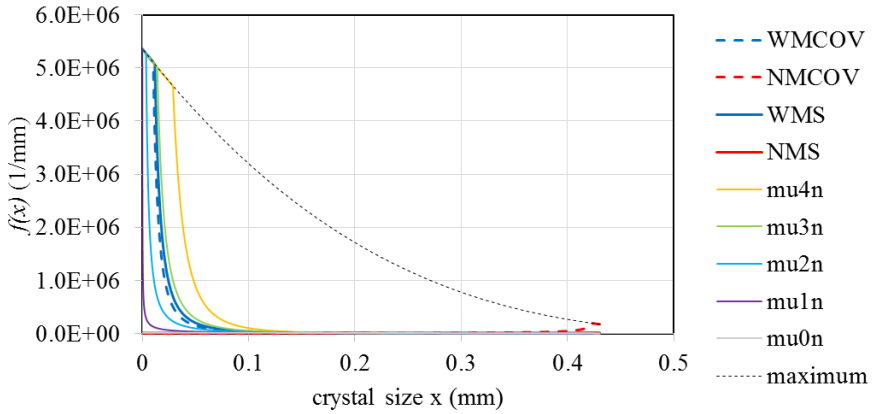

Figure 15. Crystal size distribution of the nucleus crystal for succinic acid system (3.2% seed loading).

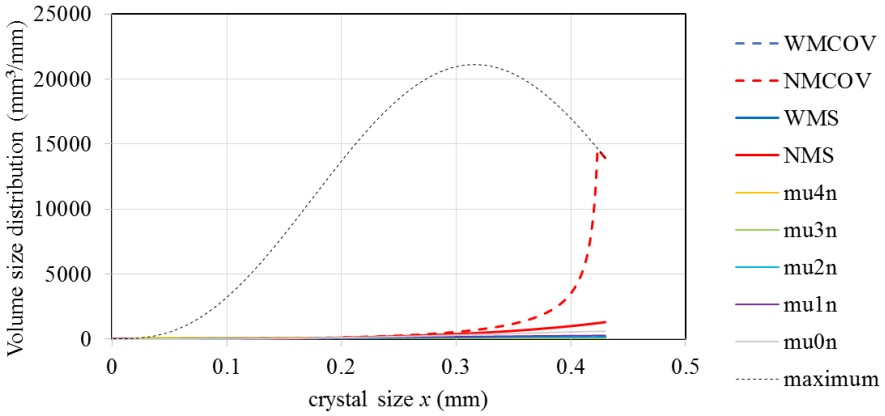

Figure 16. Volume size distribution of the nucleus crystal for succinic acid system (3.2% seed loading).

Tables

Table 1. Kinetic parameters for the three system used in this study.

		Potassium nitrate	**Succinic acid**	**Pentaerythritol**	
Variable	**Name**		**Value**		**Units**
k_b	nucleation parameter	3.47×104 (#/mm3 min)	3.09×109 (#/mm3 min)	2.47×109 (#/kg min)	-
b	nucleation parameter	1.78	4.01	3.8	dimensionless
k_g	growth parameter	6.97	3.32	3.44	mm/min
g	growth parameter	1.32	1.05	1.9	dimensionless
j	nucleation parameter (the third moment term)	1	1	0	dimensionless
t_f	total batch time	60	100	100	min
$\mu_{3s,0}$	initial third moment of the seed crystal	189.6	133.5	357	mm^3
$\mu_{3s,f}$	final third moment of the seed crystal	17064	11850	5357	mm^3
L_0	initial seed mean size	0.2	0.2	0.2	mm
L_f	final seed mean size	0.552	0.935	0.497	mm
τ_f	final tau	0.352	0.735	0.297	mm
G_{max}	growth rate constraint	0.17	0.0228	0.8	mm/min
m_{solv}	mass of the solvent	1.65	1	1	kg

Table 2. Definitions and abbreviations of the objective functions.

Objective	Abbreviation	Definition
Weight mean coefficient of variation	wCOV	$\min_{u\in U}\sqrt{\frac{\mu_{3T,f}\times\mu_{5T,f}}{\mu_{4T,f}^2}-1}$
Number mean coefficient of variation	nCOV	$\min_{u\in U}\sqrt{\frac{\mu_{0T,f}\times\mu_{2T,f}}{\mu_{1T,f}^2}-1}$
Weight mean size	WMS	$\max_{u\in U}\frac{\mu_{4T,f}}{\mu_{3T,f}}$
Number mean size	NMS	$\max_{u\in U}\frac{\mu_{1T,f}}{\mu_{0T,f}}$
The fourth moment of the nuclei	mu4n	$\min_{u\in U}\mu_{4n,f}$
The third moment of the nuclei	mu3n	$\min_{u\in U}\mu_{3n,f}$
The second moment of the nuclei	mu2n	$\min_{u\in U}\mu_{2n,f}$
The first moment of the nuclei	mu1n	$\min_{u\in U}\mu_{1n,f}$
The zeroth moment of the nuclei	mu0n	$\min_{u\in U}\mu_{0n,f}$

Table 3. Costate expressions and expressions for constants k_i for different objective functions.

Objective function	Adjoint state expression	*k* expression
$\min_{u\in U} \mu_{4n,f}$	$\psi_6(\tau) = k_1(\tau_f - \tau)^4$ $\psi_7(\tau) = k_2$	$k_1 = 1$
$\min_{u\in U} \mu_{3n,f}$	$\psi_6(\tau) = k_1(\tau_f - \tau)^3$ $\psi_7(\tau) = k_2$	$k_1 = 1$
$\min_{u\in U} \mu_{2n,f}$	$\psi_6(\tau) = k_1(\tau_f - \tau)^2$ $\psi_7(\tau) = k_2$	$k_1 = 1$
$\min_{u\in U} \mu_{1n,f}$	$\psi_6(\tau) = k_1(\tau_f - \tau)$ $\psi_7(\tau) = k_2$	$k_1 = 1$
$\min_{u\in U} \mu_{0n,f}$	$\psi_6(\tau) = k_1$ $\psi_7(\tau) = k_2$	$k_1 = 1$
$\max_{u\in U} \frac{\mu_{1T,f}}{\mu_{0T,f}}$	$\psi_6(\tau) = -k_1(\tau - \tau_f) + k_2$ $\psi_7(\tau) = k_3$	$k_1 = \frac{-1}{\mu_{0T,f}}, \quad k_2 = \frac{\mu_{1T,f}}{\mu_{0T,f}^2}$
$\max_{u\in U} \frac{\mu_{4T,f}}{\mu_{3T,f}}$	$\psi_6(\tau) = k_1(\tau - \tau_f)^4 - k_2(\tau - \tau_f)^3$ $\psi_7(\tau) = k_3$	$k_1 = \frac{-1}{\mu_{3T,f}}, \quad k_2 = \frac{\mu_{4T,f}}{\mu_{3T,f}^2}$
$\min_{u\in U} \sqrt{\frac{\mu_{3T,f} \times \mu_{5T,f}}{\mu_{4T,f}^2} - 1}$	$\psi_6(\tau) = -k_1(\tau - \tau_f)^5 + k_2(\tau - \tau_f)^4 - k_3(\tau - \tau_f)^3$ $\psi_7(\tau) = k_4$	$k_1 = \frac{1}{2\sqrt{\frac{\mu_{3T,f} \times \mu_{5T,f}}{\mu_{4T,f}^2} - 1}} \times \frac{\mu_{3T,f}}{\mu_{4T,f}^2}$ $k_2 = \frac{-1}{\sqrt{\frac{\mu_{3T,f} \times \mu_{5T,f}}{\mu_{4T,f}^2} - 1}} \times \frac{\mu_{5T,f}\mu_{3T,f}}{\mu_{4T,f}^3}$ $k_3 = \frac{1}{2\sqrt{\frac{\mu_{3T,f} \times \mu_{5T,f}}{\mu_{4T,f}^2} - 1}} \times \frac{\mu_{5T,f}}{\mu_{4T,f}^2}$
$\min_{u\in U} \sqrt{\frac{\mu_{0T,f} \times \mu_{2T,f}}{\mu_{1T,f}^2} - 1}$	$\psi_6(\tau) = k_1(\tau - \tau_f)^2 - k_2(\tau - \tau_f) + k_3$ $\psi_7(\tau) = k_4$	$k_1 = \frac{1}{2\sqrt{\frac{\mu_{0T,f} \times \mu_{2T,f}}{\mu_{1T,f}^2} - 1}} \times \frac{\mu_{0T,f}}{\mu_{1T,f}^2}$ $k_2 = \frac{-1}{\sqrt{\frac{\mu_{0T,f} \times \mu_{2T,f}}{\mu_{1T,f}^2} - 1}} \times \frac{\mu_{2T,f}\mu_{0T,f}}{\mu_{1T,f}^3}$ $k_3 = \frac{1}{2\sqrt{\frac{\mu_{0T,f} \times \mu_{2T,f}}{\mu_{1T,f}^2} - 1}} \times \frac{\mu_{2T,f}}{\mu_{1T,f}^2}$

Table 4. Values of objectives for succinic acid system with 1% seed loading.

	wCOV --	nCOV --	WMS mm	NMS mm	$\mu_{4n,f}$ mm^4	$\mu_{3n,f}$ mm^3	$\mu_{2n,f}$ mm^2	$\mu_{1n,f}$ mm	$\mu_{0n,f}$ --
wCOV	0.1704	2.2828	0.8787	0.0813	1.24×10^{3}	2.19×10^{3}	4.77×10^{3}	2.10×10^{4}	4.10×10^{5}
nCOV	0.3209	0.2983	0.6307	0.4803	1.69×10^{4}	3.25×10^{4}	6.49×10^{4}	1.35×10^{5}	2.94×10^{5}
WMS	0.1773	2.1679	0.8856	0.0759	7.01×10^{2}	1.47×10^{3}	4.21×10^{3}	2.55×10^{4}	4.99×10^{5}
NMS	0.2472	0.3934	0.7297	0.5433	1.06×10^{4}	1.78×10^{4}	3.09×10^{4}	5.59×10^{4}	1.13×10^{5}
$\mu_{4n,f}$	0.2294	1.6090	0.8688	0.0797	5.25×10^{2}	1.53×10^{3}	6.87×10^{3}	5.48×10^{4}	8.43×10^{5}
$\mu_{3n,f}$	0.1920	1.9928	0.8827	0.0756	5.72×10^{2}	1.37×10^{3}	4.71×10^{3}	3.27×10^{4}	5.97×10^{5}
$\mu_{2n,f}$	0.1773	2.1485	0.8839	0.0939	7.40×10^{2}	1.54×10^{3}	3.99×10^{3}	1.81×10^{4}	3.22×10^{5}
$\mu_{1n,f}$	0.1842	1.3572	0.8725	0.2258	1.14×10^{3}	2.17×10^{3}	4.72×10^{3}	1.36×10^{4}	1.06×10^{5}
$\mu_{0n,f}$	0.2094	0.7202	0.8433	0.4323	2.14×10^{3}	3.85×10^{3}	7.53×10^{3}	1.72×10^{4}	5.67×10^{4}